Fuel 209 (2017) 754–768

Contents lists available at ScienceDirect

Fuel

journal homepage: www.elsevier.com/locate/fuel

Full Length Article

Improvement of dual-fuel biodiesel-producer gas engine performance acting on biodiesel injection parameters and strategy

A.P. Carlucci, A. Ficarella, D. Laforgia, L. Strafella*

Department of Engineering for Innovation (DII), University of Salento, Ecotekne University Campus, Via per Monteroni, 73100 Lecce, Italy

ARTICLE INFO

Keywords:
Dual-fuel
Biodiesel
Producer gas
Injection pressure
Injection timing
Injection splitting

ABSTRACT

Dual-fuel biodiesel-producer gas combustion has shown potential in reducing nitric oxides and particulate emission levels compared to only diesel operation; however, engine overall efficiency is slightly penalized, while the main drawbacks are represented by the higher levels of total hydrocarbons and carbon monoxide emissions.

In this work, the improvements in the combustion development deriving from the splitting of the liquid fuel injection at low loads have been assessed using a 0.51 L single-cylinder research diesel engine equipped with a high pressure common rail injection system and operated in dual-fuel mode. In this case, a synthetic producer gas was used as inducted gaseous fuel, while biodiesel was used as pilot fuel.

Initially, the spray morphology was characterized in a constant-volume vessel for different values of injection duration and pressure, as well as vessel backpressure.

Then, the experimental campaign, run on the engine at 1500 rpm, was divided in two sessions. During the former, only one pilot injection of constant fuel amount (11 mm^3/cycle) was performed, the rail pressure was set equal to 500 or 1000 bar, the injection timing was varied in the range $-50 \div 5$ degrees crank angle after top dead center while the amount of gaseous fuel inducted in the cylinder was varied on three levels. During the latter, the pilot fuel amount, kept equal to the one pilot injection tests, was split in two smaller injections and the effect of the dwell between them – varied in the range $5 \div 50$ degrees crank angle – was investigated as well.

The results of the first set of experiments revealed that pilot injection timing and pressure both affect the combustion development. This resulted in sensible variations on thermal and combustion efficiencies, and therefore on fuel conversion efficiency, the last one exhibiting higher values with pilot injection timing slightly advanced respect to top dead center and lower injection pressure. In these conditions, total hydrocarbons and carbon monoxide are lowered, while nitric oxides are increased. The amount of gas demonstrated to have a secondary effect on combustion development and emissions levels at the exhaust.

Splitting pilot injection, demonstrated to be an effective way to increase fuel conversion efficiency and to reduce the levels of all the pollutant species compared to the single pilot injection strategy. Based on the extensive experimental activity described in this paper, a dwell ranging between 10 and 30 degrees of crank angle, combined with a first injection timing ranging between 35 and 20 degrees of crank angle before top dead center guarantee the highest fuel conversion efficiency and the lowest pollutants emission levels. Injection pressure confirmed to be a significant factor in affecting the combustion development, while a secondary effect was determined by the gaseous mass inducted in the cylinder.

Ultimately, pilot injection splitting demonstrated to be an effective way for improving gaseous fuel combustion in dual-fuel mode at low load (lean mixture) conditions.

1. Introduction

Worries about crude oil supplies and oil price instabilities are pushing the research towards the evaluation of alternative energy sources. Among them, biomasses appear to have promising potentials. In fact, thanks to local availability, they are considered very suitable for decentralized power and heat production. Through several available processes, biomasses can be converted in fuels more suitable for the utilization in Internal Combustion Engines (ICE) [1,2]. Among them, producer gas has drawn particular attention either as primary fuel for feeding spark ignition [3] or Homogeneous Charge HCCI Compression Ignition (HCCI) engines [4], or as secondary fuels in dual-fuel engines [5–8]. In particular, dual-fuel combustion, consisting in the introduction of gaseous fuel into the combustion chamber and its ignition by

* Corresponding author.
E-mail address: luciano.strafella@unisalento.it (L. Strafella).

http://dx.doi.org/10.1016/j.fuel.2017.07.100
Received 24 February 2017; Received in revised form 28 June 2017; Accepted 5 July 2017
Available online 04 August 2017

Nomenclature

ABDC	After Bottom Dead Center
ATDC	After Top Dead Center
BBDC	Before Bottom Dead Center
BP	Vessel backpressure
BTDC	Before Top Dead Center
CAD	Crank Angle Degrees
CO	Carbon Monoxide
COV_{IMEP}	Coefficient of Variance of indicated mean effective pressure
$(dp_{cyl,abs}/dCAD)_{max}$	Maximum rate of cylinder pressure rise
dw	Dwell between the two injections beginning
ES	Energy Substitution rate
ET	Injection duration
HCCI	Homogeneous charge compression ignition
HRR	Heat Release Rate
ICE	Internal Combustion Engine
IMEP	Indicated Mean Effective Pressure
NO_x	Nitric Oxides
PM	Particulate Matter
Q_p	Biodiesel amount injected per cycle
SOI	Start Of Injection
SOI_p	Biodiesel pilot injection timing
THC	Total Hydrocarbons
TDC	Top Dead Center
p_{in}	Engine intake pressure
p_rail	Biodiesel rail injection pressure
T_{in}	Engine intake temperature
A_{ht}	Instantaneous transfer surface area
$H_{i,biod}$	Biodiesel lower calorific value
$H_{i,gf}$	Gaseous fuel lower calorific value
P_i	Engine Indicated power
Q_{net}	In-cylinder net heat released
Q_w	Heat transferred to the cylinder walls
T	Instantaneous bulk temperature in the cylinder
T_w	Temperature of the cylinder walls
V	Instantaneous cylinder volume
h_c	Heat transfer coefficient
k	Specific heat ratio
$\dot{m}_a$	Intake air mass flow rate
$\dot{m}_{biod}$	Biodiesel mass flow rate
$\dot{m}_{gf}$	Gaseous fuel mass flow rate
n	Engine speed
n_R	Number of crank revolutions for each power stroke
$p_{cyl,abs}$	Absolute cylinder pressure
η_b	Combustion efficiency
η_c	Thermal efficiency
η_f	Fuel Conversion Efficiency Referred to the Indicated Power

means of a small amount of diesel oil or similar fuel, is particularly attractive as it can be implemented, with relatively simple modifications using a traditional diesel engine. Many works have shown that in this way it is possible to obtain a significant reduction of nitric oxides (NO_x) and particulate matter (PM) emissions keeping constant or only slightly penalizing the engine overall efficiency [9]. Drawbacks are the higher levels of total hydrocarbons (THC) and carbon monoxide (CO) measured at the exhaust believed to be due to both the overleaning of the air-gaseous fuel mixture at low loads, and the mixture escaping during the valve overlap.

Combustion and related emission levels in dual-fuel engines can be controlled in many ways. The composition of gaseous fuel, for example, plays an important role, as demonstrated in [10–13] as well as the utilization of biodiesel or blends of biodiesel and standard diesel as pilot fuel [14–16]. The Energy Substitution rate (ES) is also a very important factor, as demonstrated, for example, in [17,18] as well as boost pressure [4,19], intake temperature [4,20] and exhaust gas recirculation [21]. Pilot injection parameters, like injection pressure, timing, quantity, and number of injections, play a fundamental role in controlling combustion development and consequently pollutant emission levels in dual-fuel engines as reported in [22–29]. The same analysis, in terms of advance, pressure and fuel quantity related to pilot injection, has been done on an engine fed with biodiesel and simulated producer gas [6]. Afterwards, the pilot injection has been split into two smaller “split” injections, the first injection aiming as usual at igniting the producer gas, while the second trying to “boost” the combustion of the producer gas also during the late combustion phase [7]. It was concluded that splitting the injection has a major influence on both combustion development and NO_x, CO and THC tailpipe emissions, beneficial when the dwell between injections is in the range 10–30 degrees crank angle. With the dwell ranging in this interval, also the fuel conversion efficiency is increased. Data presented in [7] have been all obtained injecting the pilot fuel at 500 bar. This injection pressure is relatively low if compared to the current state of the art of diesel injection systems. Injecting the pilot fuel at a higher pressure would contribute to better diffuse it into the combustion chamber, so obtaining a more complete combustion of the gaseous fuel even at low loads. Despite the literature concerning the dual-fuel combustion is very rich, it is difficult to find works dealing with the effect of the pressure at which the pilot fuel is injected. Therefore, in the first part of this work, the spray morphology of pilot injections varying the injection pressure has been characterized on a constant-volume vessel for different values of injected amount and vessel backpressure. Then, a single cylinder diesel engine has been run at 1500 rpm and fed with a constant amount of biodiesel and variable amount of simulated producer gas, for this reason referred to as “syngas” in the following. The effect of pilot injection pressure and timing - the latter varied on a wide range - and producer gas quantity has been evaluated in the case of a single pilot injection and when the pilot injection is split into two split injections, with variable dwell, on cylinder pressure, heat release rate (HRR), combustion and fuel conversion efficiency and NO_x, THC and CO emission levels at the exhaust.

2. Experimental setup

2.1. Characterization of the spray morphology

The morphology of the liquid phase of the spray has been characterized in conditions representative of the actual operation used during the experimental campaign on the engine in order to support the analysis of data. The tests on sprays have been performed injecting the biodiesel into a constant-volume steel chamber using a 5-holes common rail injector (model Bosch 0445110266-825) characterized by a nozzle diameter equal to 0.170 mm, a cone angle equal to 142° and the cone axis coincident with the axis of the injector body. The constant-volume vessel was equipped with quartz optical accesses in order to allow the spray lighting with external light source, as well as the injection event images recording. Once the rail pressure had reached the desired value – acting on the duty-cycle of the electrovalve on the return line of the high pressure pump – a signal was generated, triggering both the injection event (through a homemade injector driving board, see [30] for more details) and the images acquisition through a MEMRECAM GXlink camera. The images have been acquired with a sample rate of 20 kHz and a 308 × 304 pixel resolution exposing the spray to an external light source in order to increase the contrast between the spray and the chamber background. The images so acquired were converted in black

and white in order to calculate the temporal evolution of penetration (length of the segment joining the tip of the liquid phase to its nozzle exit) and shape ratio (ratio between the penetration and the maximum depth of the liquid phase in the direction orthogonal to the penetration) for each spray. More details about the post-processing of the spray images are reported in [30]. During the experimental campaign described in the present paper, the injection duration, rail pressure, pressure into the constant-volume chamber (backpressure) and dwell between the two injections (in case of injection split in two injections) have been varied on a range of values representative, as previously said, of the actual operation used during the experimental campaign on the engine. Table 1 summarizes the experimental plan for the liquid phase characterization, specifying the levels assigned to each variable during the experiments. The total amount of fuel injected during each test (either performing a single injection or two injections) was kept constant and equal to 11 mm^3.

2.2. Experiments on single cylinder research engine

A single cylinder, 4-stroke, common-rail Diesel research engine (AVL model 5402) was used to analyze the effect of biodiesel injection parameters and strategy on the biodiesel-producer gas dual-fuel combustion. The technical features of the engine are reported in Table 2, while in Fig. 1 the scheme of the experimental layout is reported. The gaseous fuel has been introduced in the intake duct of the engine by means of an injector consisting of an automatic poppet valve, with contrast spring, actuated by the gaseous fuel introduced by a solenoid valve in an small accumulation volume [27]. The solenoid valve was actuated using a duty cycle D = 50% with a frequency of 30 Hz. During the tests, the injector has been positioned along the intake duct, at a distance of about 400 mm from the cylinder axis, so that a homogeneous gaseous air-fuel mixture was obtained before inducting it into the cylinder. The mixture entered the cylinder through an intake port shaped to provide the flux with a swirl bulk motion.

The Machinery Laboratory at University of Salento is equipped with a mixing system for gaseous species, whose operative scheme is presented in Fig. 1. This system allows to obtain a gaseous mixture of CO, H_2 and N_2; the percentage of each species can be arbitrarily fixed. The mixture, whose pressure can vary in the range 0–10 barg, is first stored in a cylinder and then delivered to the engine. During the tests, the composition of the syngas was kept constant (see Table 3); the composition was chosen similar to the composition of the producer gas obtained by the gasification of lignocellulosic biomass in a gasifier-ICE system developed by a local company [31].

A pilot injection of biodiesel was used as ignition source for the gaseous fuel. The biodiesel injection system was equal to the one used for spray morphology characterization on the constant-volume vessel. The main specifications of the biodiesel used during tests are reported in Table 3.

The experiments carried out on the engine are divided in two sessions (see Table 4). In the first session, during which only one pilot injection quantity Q_p of 11 mm^3/cycle was performed, the effect of the rail pressure (p_rail) and pilot injection timing (SOI_p) has been studied for different amount of syngas $\dot{m}_{gf}$ (and different related values of ES, reported in Table 4) feeding the engine. During the second session, the effect of pilot injection splitting was added. The dwell (i.e. the angular or time interval) between the two injections beginning was varied on levels reported in Table 4, while the amount of fuel totally injected during the two injections was kept equal to that characterizing tests with only one pilot injection. Referring to the last cell identified intersecting the last row and last column of Table 4, the first number of each label (SOI) is the injection timing of the first injection, while the numbers reported in round bracket, are the dwells tested for that particular injection timing of the first injection. For example, the label −50/(30 – 40 – 50) indicates that the dwells of 30, 40 and 50 CAD have been tested for a first injection timing (SOI) of −50 CAD After Top Dead Center (ATDC).

During tests presented in this paper, the average mass flow rate of gaseous fuel was varied on the levels reported in Table 4 in order to simulate three fueling conditions.

During the experiments, data acquisition started only when the engine had reached steady operating conditions in particular in terms of engine speed, torque and cooling water temperature. The in-cylinder pressure was measured with a piezoelectric pressure sensor AVL QC33C triggered through an AVL angle encoder model 364 C every 0.2 CAD. Furthermore, the pegging of the in-cylinder pressure was done through the absolute pressure measurement in the intake duct. The absolute pressure transducer was a Kistler piezoresistive sensor type 4045A2. The in-cylinder pressure signals (absolute cylinder pressure, $p_{cyl,abs}$) related to 25 consecutive cycles were stored and then averaged. The accuracy of the pressure transducer was less than ± 0.5 bar, while the sensitivity shifts and the range error of the pressure amplifier (AVL model 3066A01) was less than 1%. The measurement error in the analogue/digital data conversion and acquisition has been evaluated equal to 0.3%.

The gross Heat Release Rate (HRR) was then calculated as:

$$HRR = \frac{dQ_{net}}{d(CAD)} + \frac{dQ_w}{d(CAD)} \tag{1}$$

The term $\frac{dQ_{net}}{d(CAD)}$ has been estimated based on the single zone simplified model:

$$\frac{dQ_{net}}{d(CAD)} = \frac{k}{k-1} p_{cyl,abs} \frac{dV}{d(CAD)} + \frac{1}{k-1} V \frac{dp_{cyl,abs}}{d(CAD)} \tag{2}$$

where k, ratio between constant pressure and constant volume specific heats, has been assumed equal to 1.38, while V is the instantaneous cylinder volume. The term $\frac{dQ_w}{d(CAD)}$, accounting for the heat transfer through the cylinder walls, has been estimated as:

$$\frac{dQ_w}{d(CAD)} = A_{ht} h_c (T - T_w) \tag{3}$$

where A_{ht} is the instantaneous exchange area of the combustion chamber, T is the instantaneous bulk temperature in the cylinder estimated with the state equation of the perfect gases, T_w is the temperature of the cylinder walls considered constant and equal to 600 [K], mean value among cylinder head, piston and cylinder walls, while the heat transfer coefficient h_c was estimated as proposed by Woschni [32]. The maximum error in this calculation, due to the errors in the pressure measurement, is around 2%. Based on cylinder pressure, it was possible to estimate the indicated power P_i supplied by the engine:

$$P_i = \oint_{cycle} p_{cyl,abs} dV \frac{n}{n_R} \tag{4}$$

where n is the engine speed while n_R (= 2 in this case) is the number of crank revolutions for each power stroke. The biodiesel average mass flow rate was measured by means of a AVL 733S Fuel Balance, characterized by a maximum measurement error in the testing conditions

Table 1
DoE for the spray characterization (single and split injection).

Description	Abbreviation [m.u.]	Tested values
Experimental DoE – Spray characterization (single injection)		
Rail pressure/Injection duration	p_rail [bar]/ET [μs]	500/370; 1000/210
Backpressure	BP [bar]	7 – 11 – 22 – 40
Experimental DoE – Spray characterization (split injection)		
Rail pressure/Injection duration	p_rail [bar]/ET [μs]	500/230; 1000/140
Backpressure	BP [bar]	7 – 11 – 22 – 40
Dwell between the two injections beginning	dw [ms]	0.6 – 1.1 – 1.7 – 2.2 – 3.3 – 4.4 – 5 – 5.6

Table 2
Main specifications of single cylinder diesel engine.

Specification	Nominal value/description	
Maximum power	18 kW	
Bore	85 mm	
Stroke	90 mm	
Connecting rod length	148 mm	
Compression ratio	17.1:1	
Combustion chamber	bowl with valve pockets and flat head	
Injection system	common-rail	
Max. Injection pressure	1300 bar	
Valve timing	Opening	Closing
Intake	13.5 CAD BTDC	46.5 CAD ABDC
Exhaust	51.5 CAD BBDC	16.5 CAD ATDC

Table 3
Main specifications of biodiesel and syngas.

Fuel	Property	Value
Biodiesel	Water content	205 mg/kg
	Viscosity@40 °C	4.458 mm^2/s
	Flash point	169 °C
	Cetane number	52
	Density@15 °C	883.5 kg/m^3
	Total glycerine	0.2% m/m
	Methanol	0.03% m/m
	Methyl ester	97.3% m/m
	Lower Calorific Value	36.5 MJ/kg
	Estimated air-to-fuel stoichiometric ratio	14.5
Syngas and Constituents Properties	N_2 purity	> 99.9995%
	H_2 purity	> 99.995%
	H_2 Lower Calorific Value	142 MJ/kg
	CO purity	> 99.90%
	CO Lower Calorific Value	18 MJ/kg
	Syngas formulation	60%vol. N_2 20%vol. H_2 20% vol. CO
	Estimated Lower Calorific Value	26.2 MJ/kg
	Estimated air-to-fuel stoichiometric ratio	1.209

equal to 3%.

The flow rate of the syngas is measured through a thermal flow controller manufactured by Aalborg Instruments and Controls Inc., model DFC 36. Furthermore, in order to take into account the composition of the flowing gas mixture, the measured value has been corrected because the controller was calibrated with nitrogen. In order to correct this value, temperature and pressure of the flowing mixture have been continuously monitored through a pressure gauge and a K-type thermocouple. The measurement error of the different instruments is reported in Table 5. The measurement of the fuels mass flow rate allowed to estimate the fuel conversion efficiency referred to the indicated power P_i:

$$\eta_f = \frac{P_i}{\dot{m}_{biod} H_{i,biod} + \dot{m}_{gf} H_{i,gf}} \quad (5)$$

where $H_{i,biod}$ and $H_{i,gf}$ are the lower calorific value respectively of biodiesel and syngas (see Table 2) while $\dot{m}_{biod}$ is the mass flow rate of biodiesel.

Gaseous regulated pollutant emission such as NO_x, THC and CO were measured with an AVL AMAi 60 emission analyzer. In particular, NO_x levels were measured through a ChemiLuminescence Detector (CLD) analyzer, whose operation is based on the measurement of the light emitted during the oxidation of nitrogen oxide, NO, with ozone, O_3. THC levels have been measured through a Flame Ionization Detector (FID) analyzer, the operating principle being based on the ionization of the carbon atoms through a hydrogen flame immersed in an electric field. Finally, CO levels have been measured through an Infrared Detector (IRD) analyzer; the operating principle is based on the measurement of a non-dispersive infrared radiation, correlated to the concentration of the component to be measured. Each analyzer is characterized by having a linearity ≤2% of reading. All emission levels measurements have been converted in g/kWh referred to indicated power.

PM emissions have not been measured during tests; however, they are not considered a main issue for the following reasons. On one hand, the mixture preparation (mainly premixed), is expected to lead to few rich zones, believed as the zone where PM is generated from. On the other hand, the injection splitting usually determines a better utilization of the air in the cylinder [33–36], especially in the engines equipped with swirling intake port, as the one used in the present study. Therefore, the injection splitting, investigated in this work, is reasonably expected to determine a reduction of PM emissions, already lowered thanks to the substitution of diesel fuel with syngas. The measured experimental parameters and their accuracies are summarized in Table 5.

3. Results and discussion

3.1. Spray morphology

In Fig. 2 the morphological characterization of biodiesel pilot sprays is presented. In particular, for different backpressures reported on the

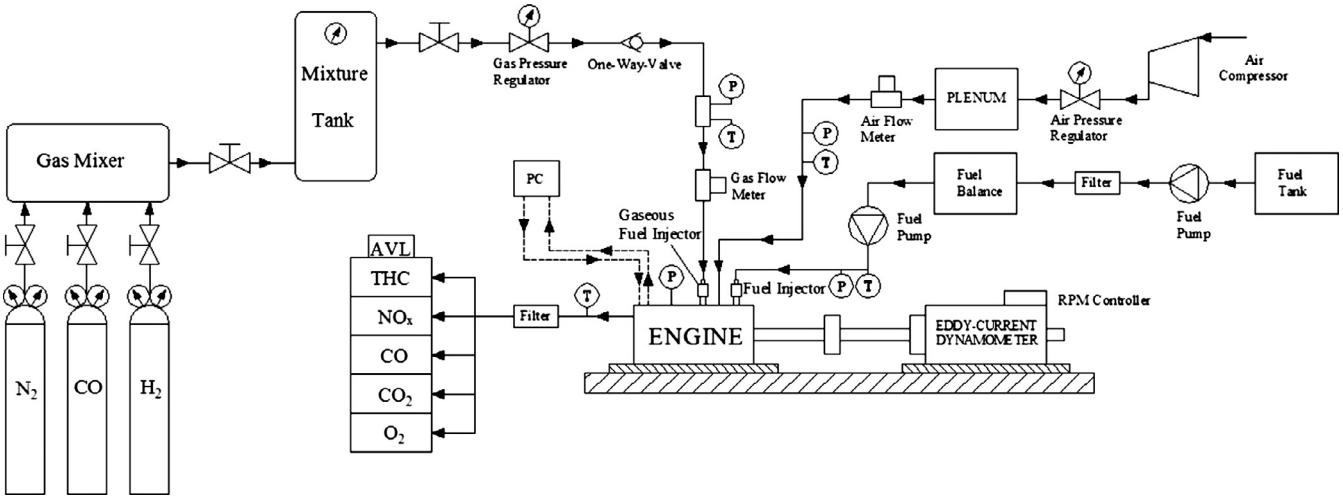

Fig. 1. Experimental setup for tests on diesel engine.

Table 4
Factors and corresponding levels varied during tests.

Description	Abbreviation	Tested levels
Experimental setup – General		
Syngas mass flow rate	$\dot{m}_{gf}$	0.36 [kg/h] (ES = 35%) − low fueling level 0.68 [kg/h] (ES = 50%) − medium fueling level 1.15 [kg/h] (ES = 65%) − high fueling level
Biodiesel amount injected per cycle	Q_p	11 [mm^3/cycle]
Engine speed	*n*	1500 [rpm]
Experimental setup – Session 1		
Biodiesel rail injection pressure	p_rail	500 – 1000 [bar]
Biodiesel pilot injection timing	SOI_p	−50/−35/−20/−10/0/5 [CAD ATDC]
Experimental setup – Session 2		
Biodiesel rail injection pressure	p_rail	500 – 1000 [bar]
Timing of the first biodiesel injection/dwell between beginning of first and second biodiesel injections	SOI/dwell	−50 [CAD ATDC]/(30 – 40 – 50) [CAD] −35 [CAD ATDC]/(15 – 25 – 35 – 40 – 45) [CAD] −20 [CAD ATDC]/(10 – 20 – 25 – 30) [CAD] −10 [CAD ATDC]/(10 – 15 – 20) [CAD] 0 [CAD ATDC]/(5 – 10) [CAD] 5 [CAD ATDC]/(5) [CAD]

Table 5
Accuracies of various measurement instruments.

Measured parameters	Unit	Accuracy
Biodiesel flow rate	kg/h	± 0.12% of reading
Syngas mass flow rate	kg/h	± 0.05 kg/h
Air mass flow rate	kg/h	≤1% of reading
Temperatures	°C	≤1% of reading
Cylinder pressure	bar	≤ ± 0.5 bar
Intake pressure	bar	≤ ± 0.006 bar
THC emissions	ppm	≤2% of reading
NO_x emissions	ppm	≤2% of reading
CO emissions	ppm	≤2% of reading

left side: Fig. 2a shows the penetration, as a function of time, average of the penetration of the five sprays, and the related standard deviation - calculated over the five sprays - when injecting at 500 [bar] for a duration of 370 [μs]; Fig. 2b, c and d compare respectively the average penetration, the shape factor and the temporal evolution of the spray shape obtained varying the rail pressure and the injection duration in order to keep constant the injected amount.

Fig. 2a indicates that increasing backpressure sensibly reduces the dispersion (standard deviation) of penetration, and consequently shape factor, among the five plumes. From Fig. 2b it can be argued that spray penetration is somewhat independent of injection pressure, as already described in [37]; moreover, as well established in literature, the maximum penetration of the jet decreases as the backpressure

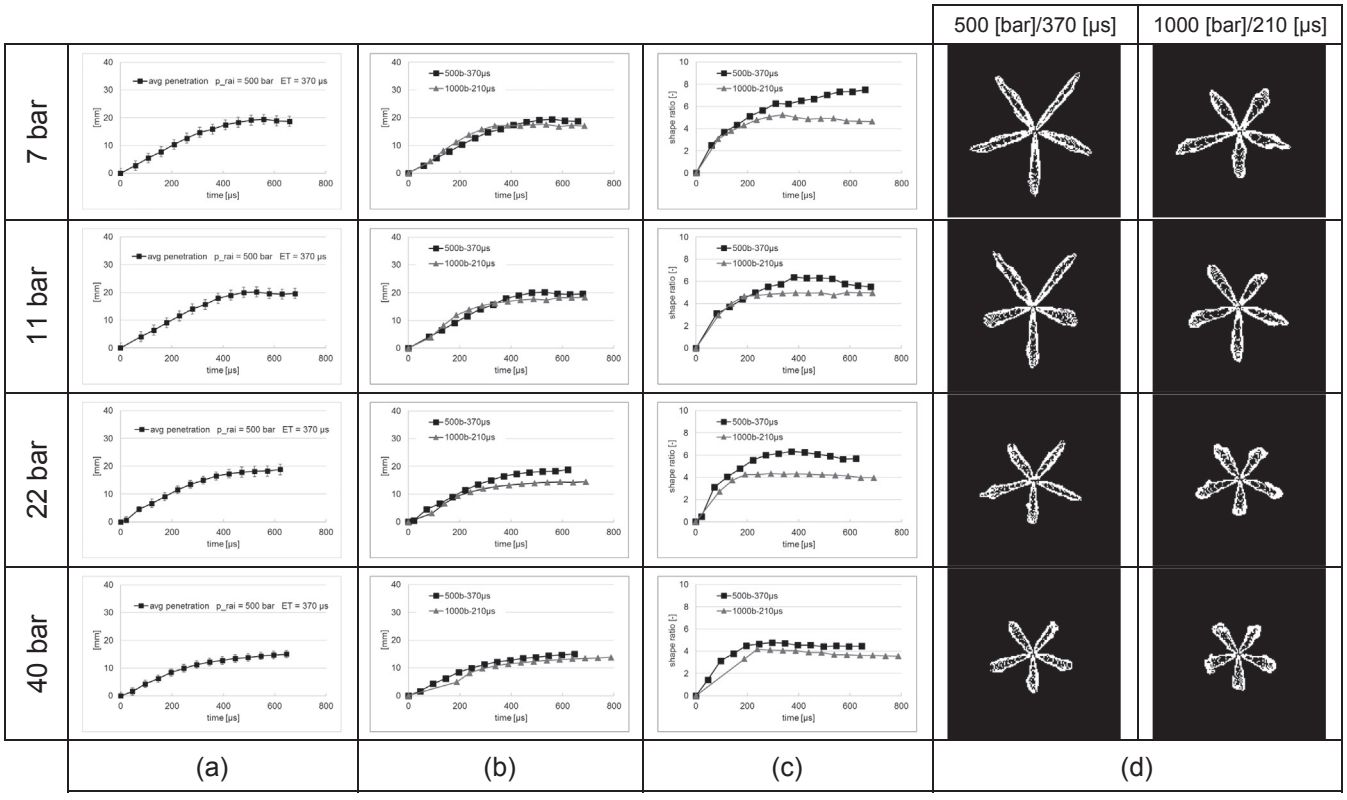

Fig. 2. Morphological characterization of biodiesel pilot sprays: a) average penetration and standard deviation vs time (p_rail = 500 [bar], ET = 370 [μs]; b) spray average penetration; c) spray shape factor; d) spray shape.

increases. Furthermore, for all the backpressure values tested, the jet penetration never exceeds 20 mm; this means that, in the actual injection conditions, neglecting the autoignition of the spray, the penetration of the liquid phase will cover only about one half of the maximum available radial distance, equal to half the cylinder bore. This dimension is roughly equal to that of the bowl, therefore, it is deducible that the spray will not impinge the walls of the bowl itself. The utilization of the air trapped into the cylinder will be therefore penalized. These comments will be useful in supporting the analysis of the results related to the burning of these sprays. Although a granulometric characterization of the jet has not been done, it is likely to expect that the spray injected at 1000 bar is dispersed more finely than at 500 bar. The shape factor is higher with lower injection pressure, as shown in Fig. 2c, since the bigger droplets obtained with a lower injection pressure determines a lower influence of the viscous forces exchanged between droplets and air on the droplets trajectory.

Splitting the injection (and thus reducing the amount introduced for single injection event), both the penetration and the shape factor are slightly reduced compared to the case with single injection. In this case too, increasing the injection pressure determines a reduction of shape factor while, to a first approximation, p_rail has not effect on penetration; moreover, the increase of the backpressure significantly reduces, in this case too, the dispersion of the penetration curves with the respect to the average penetration and shape factor of the individual sprays. The dispersion values determined on penetration and on the shape factor do not vary significantly between single and split injections.

3.2. Effect of injection pressure and gaseous fuel amount on combustion development

From now on, results referring to tests performed with low, medium and high fueling rate of syngas will be labeled as “low”, “medium” and “high”. Data obtained performing only pilot injection will be labeled as “bio”. Figs. 3 and 4 show the HRR histories calculated on the basis of cylinder pressure measured at high syngas fueling rate for different pilot timing (varied from −50 CAD ATDC up to 5 CAD ATDC), when pilot injection pressure is equal to 500 bar (Fig. 3) and 1000 bar (Fig. 4). Tests have been run injecting always the same amount of gaseous fuel ($\dot{m}_{gf}$ = 29 g/cycle) and biodiesel (Q_p = 11 mm^3/cycle, corresponding to an energizing time equal to 370 and 210 μs respectively at p_rail = 500 and 1000 bar). The obtained biodiesel/air/gaseous fuel mixture was characterized by an overall air and fuel (biodiesel + gaseous fuel) excess-air ratio equal to about 3, and by an estimated stoichiometric air-gaseous fuel ratio equal to 1.2. Comparing these figures, it can be observed that, performing the pilot injection close to TDC, a higher injection pressure leads to a premixed-like combustion, while, decreasing the injection pressure, it is also visible a second stage combustion during the expansion stroke. Advancing the injection up to −50 CAD ATDC, on the contrary, determines a totally different behavior: in fact, with a lower injection pressure, the combustion exhibits a premixed-like development, while increasing the injection pressure, a slower combustion is observed, sensibly different from the premixed-like behavior. This is thought to be due to the overleaning of the mixture, resulting from a high injection pressure and a very advanced SOI_p leading to a longer ignition delay and a more advanced combustion [7].

The behavior of the ignition delay and HRR peak are synthesized in Figs. 5 to 9. Fig. 5 plots the ignition delay for different SOI_p and p_rail without introducing syngas, while in Fig. 6 data referring to the high syngas fueling rate are reported. Compared to SOI_p, p_rail has a minor effect on ignition delay, although, interestingly, its effect changes if the injection is very advanced. In these conditions, in fact, a high injection pressure determines a longer ignition delay, while, retarding the injection, a lower injection pressure leads to a longer ignition delay. This result too can be related with the overleaning of the mixture and keeping in mind that a higher injection pressure determines smaller droplets. When the pilot liquid is injected close to TDC, smaller droplets leads to a reduction of ignition delay, as the preignition phenomena in these conditions are governed by physical processes. On the contrary, for very advanced injections, where chemical kinetics time constants govern the preignition phenomena, a higher injection pressure, still determining smaller droplets, contribute to further overleaning the mixture in the pilot zone, therefore retarding its ignition. This is confirmed in Figs. 7 and 8, where HRR peaks corresponding to the early combustion phase are reported for different SOI_p and p_rail, and different amounts of syngas fueling rates. It can be noticed that the behavior of the HRR peak is concordant with that of the ignition delay as far as pilot injection is not much advanced. In this case, however, the very long ignition delay leads to the overleaning of the mixture and a slower combustion, in particular when high p_rail is adopted and so a better spray atomization is obtained. p_rail and syngas fueling rate do not affect HRR peak angle (also reported in Figs. 7 and 8) that usually results advanced with advanced SOI_p.

Comparing Figs. 5 and 6 the effect of syngas on ignition delay can be analyzed. With the syngas, the ignition delay is generally decreased; moreover, injecting at 1000 bar leads to an ignition delay always lower than at 500 bar. The effect cannot be attributed to a different value of specific heat, since the value is similar between gaseous mixture and air. It could be argued that the effect is related to the heat exchanged with the cylinder walls during the filling phase, higher when the gaseous fuel is burned in addition to pilot fuel. Fig. 9 reports the behavior of the ignition delay for different amounts of syngas: as visible, the effect of the variation of syngas is marginal, therefore the trend in Fig. 6 cannot be explained with the variation of the heat exchanged with the cylinder walls during the filling phase. Moreover, looking at Figs. 7 and 8, increasing the amount of syngas leads to an increase of the fuel burning during the “premixed” combustion phase, without varying the angle in which this combustion takes place. Therefore, it must be concluded that the ignition delay with syngas (Fig. 6) is dominated by the concentration of reactant species.

Finally, in Fig. 10, the effect of injection pressure on both CA_50 (combustion position) and CA_90 - CA_10 (combustion duration) is highlighted. This plot is representative of the trends observed for every value of syngas introduced into the combustion chamber and even in absence of syngas. The combustion duration is always lower with higher injection pressure, thanks to the faster combustion obtained with smaller droplets of biodiesel. Concerning CA_50, Fig. 10 first reveals that, progressively advancing pilot injection, an advance of CA_50 is firstly observed, followed by a “plateau”, indicating that a further

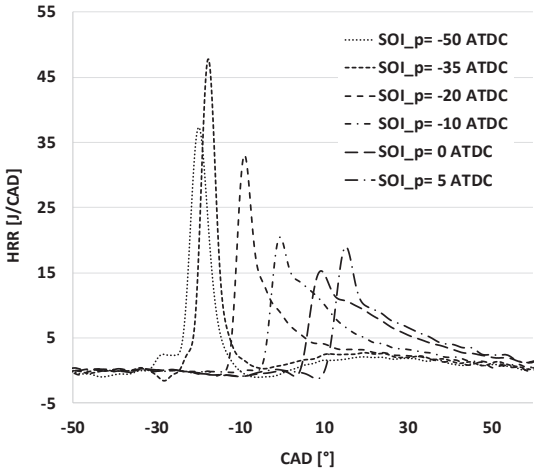

Fig. 3. Heat Release Rate versus crank angle for different pilot injection timings with p_rail = 500 bar: 1500 rpm, p_{in} = 129 kPa, T_{in} = 28 °C, Q_p = 11 mm^3/cycle (high syngas fueling rate).

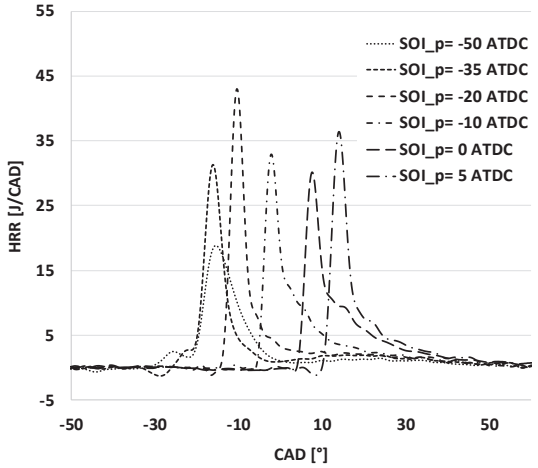

Fig. 4. Heat Release Rate versus crank angle for different pilot injection timings with p_rail = 1000 bar: 1500 rpm, p_{in} = 129 kPa, T_{in} = 28 °C, Q_p = 11 mm^3/cycle (high syngas fueling rate).

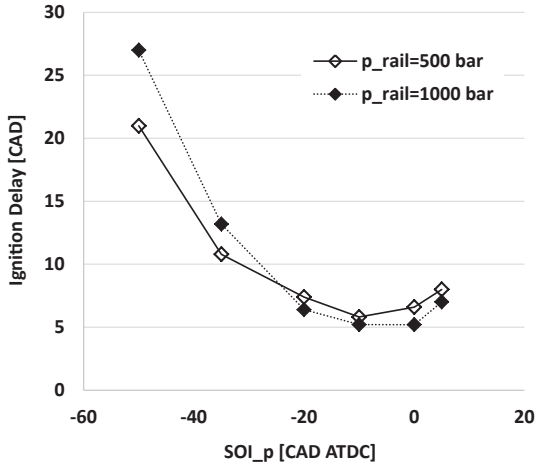

Fig. 5. Ignition delay versus pilot injection timing for two different injection pressure values: 1500 rpm, p_{in} = 129 kPa, T_{in} = 28 °C, Q_p = 11 mm^3/cycle (only biodiesel).

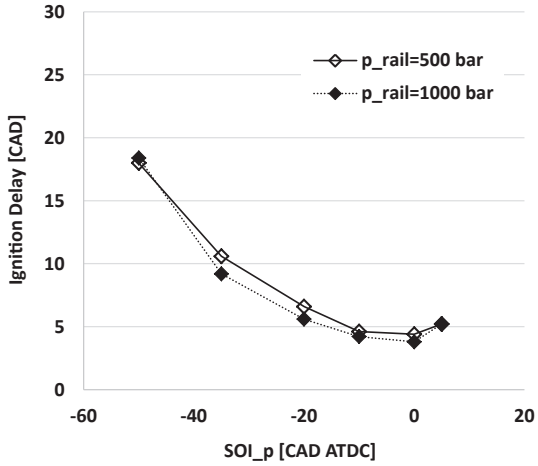

Fig. 6. Ignition delay versus pilot injection timing for two different injection pressure values: 1500 rpm, p_{in} = 129 kPa, T_{in} = 28 °C, Q_p = 11 mm^3/cycle (high syngas fueling rate).

advance of the center of combustion cannot be obtained simply acting on SOI_p. The injection pressure also affects CA_50 behavior: with SOI_p ranging between −35 and 5 CAD ATDC, a higher injection pressure

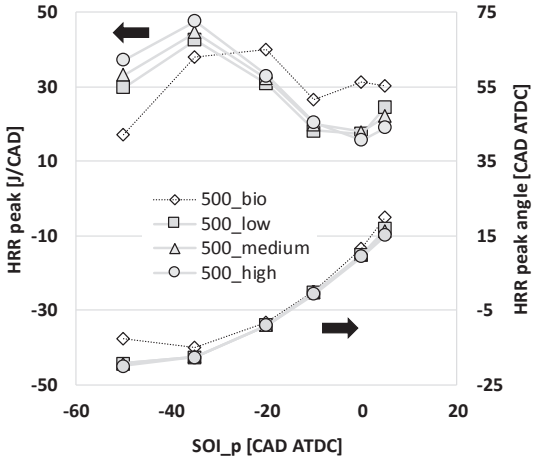

Fig. 7. HRR peak versus pilot injection timing for different syngas load with: p_rail = 500 bar, 1500 rpm, p_{in} = 129 kPa, T_{in} = 28 °C, Q_p = 11 mm^3/cycle.

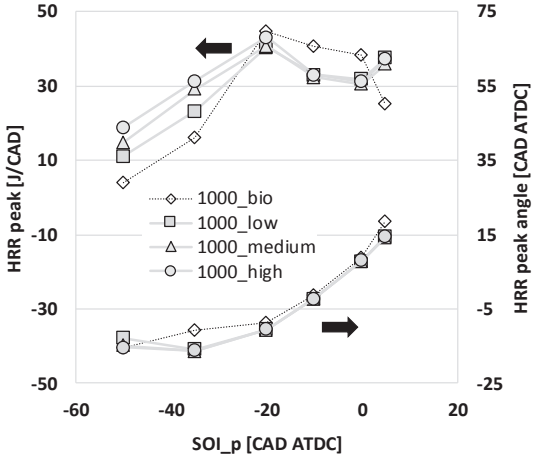

Fig. 8. HRR peak versus pilot injection timing for different syngas load with: p_rail = 1000 bar, 1500 rpm, p_{in} = 129 kPa, T_{in} = 28 °C, Q_p = 11 mm^3/cycle.

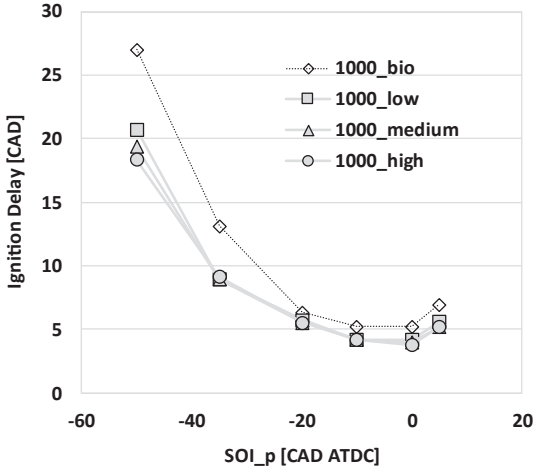

Fig. 9. Ignition delay versus pilot injection timing for different syngas load with: p_rail = 1000 bar, 1500 rpm, p_{in} = 129 kPa, T_{in} = 28 °C, Q_p = 11 mm^3/cycle.

determines a combustion position more advanced; further advancing pilot injection, a higher injection pressure determines a combustion position more retarded. As previously underlined, this effect could be due to an excessive overleaning of the mixture preparation due to long ignition delay and smaller droplets of liquid fuel.

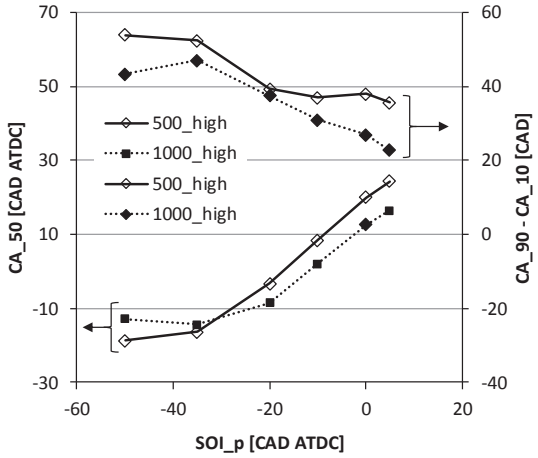

Fig. 10. CA50 and CA90-CA10 versus pilot injection timing for two different injection pressure values: 1500 rpm, p_{in} = 129 kPa, T_{in} = 28 °C, Q_p = 11 mm^3/cycle (high syngas fueling rate).

It is expected that the overall combustion duration and position both affect the conversion efficiency, η_f. However, in the tested operating conditions, the conversion efficiency can be determined either by the pilot timing and by the completeness of the combustion. The high mixture overleaning, accentuated performing the pilot injection too early or too late, together with the use of a fuel characterized by a low calorific value, are factors that can determine, as will be seen, a low combustion efficiency, defined as:

$$\eta_b = 1 - \frac{\sum x_i H_{i,i}}{\left(\frac{\dot{m}_{biod} H_{i,biod} + \dot{m}_{gf} H_{i,gf}}{\dot{m}_a + \dot{m}_{biod} + \dot{m}_{gf}}\right)} \tag{6}$$

in which x_i is the mass fractions of CO, H_2, HC and PM measured at the exhaust, $H_{i,i}$ the related lower calorific values, and $\dot{m}_a$ is the air mass flow rate at engine inlet. Because the composition of HC in the exhaust, and thus their $H_{i,i}$, are not known, the combined mass-fraction-weighted H_i of biodiesel and syngas has been used to represent the lower calorific value of HC. Moreover, because gravimetric PM was not measured, it was not considered in the combustion efficiency calculations. The efficiency of the thermodynamic cycle, namely the thermal efficiency, was calculated as:

$$\eta_c = \frac{\eta_f}{\eta_b} \tag{7}$$

In Figs. 11 and 12, the behavior of η_c, η_b and η_f are reported varying SOI_p, p_rail and the amount of syngas introduced. Analyzing the behavior of the thermal efficiency η_c (Figs. 11a and 12a) it is visible how it significantly decreases advancing of delaying the pilot injection. Such expected behavior is determined, in the first case, by a too early ignition, even in the compression phase, of the pilot fuel and, as a result, of the gaseous mixture (see also Figs. 2 and 3); in the second case, on the other hand, the heat release takes place during the expansion phase and this does not allow an optimal use of the heat released from the fuel. The cycle efficiency η_c weakly depends also on the quantity of gaseous fuel introduced, and increases increasing the quantity, probably due to the higher temperatures reached in the combustion chamber. Finally, a lower injection pressure allows the achievement of higher η_c.

Combustion efficiency η_b (Figs. 11b and 12b) shows the same decreasing behavior either advancing or retarding SOI_p, marginally affected by the injection pressure. This trend too can be justified considering that a too advanced injection causes an overleaning that makes the complete fuel combustion difficult.

Fuel Conversion Efficiency η_f values are finally reported in Figs. 11c and 12c. This behavior is, again, qualitatively in agreement with what reported in literature [28]. It consists in an increasing trend first and successively in a decreasing trend retarding the injection timing. Since the fuel introduced into the cylinder is always the same, then the behavior of the fuel conversion efficiency related to different syngas fueling rates coincides with the behavior of Indicated Mean Effective Pressure (IMEP).

In Figs. 13 and 14, the effect of SOI_p on the Coefficient of Variance of IMEP (COV_{IMEP}) is shown for different syngas fueling rates, respectively when pilot fuel is injected at 500 and 1000 bar. It is visible that COV_{IMEP} always assumes values ranging between 0.5% and 2%; as a first approximation, it can be also concluded that SOI_p and syngas fueling rate have not a strong effect on COV_{IMEP}. Comparing the two figures, it can be concluded that increasing injection pressure leads to a slight increase of COV_{IMEP}.

In Figs. 15 and 16, the effect of SOI_p on the maximum rate of pressure rise $(dp_{cyl,abs}/dCAD)_{max}$ is shown for different fueling rates, respectively when pilot fuel is injected at 500 and 1000 bar. With the addition of syngas, the maximum rate of pressure rise slightly decreases with retarded pilot injections, while slightly increases with advanced pilot injections. Comparing the two figures, it can be also concluded that increasing injection pressure leads to a slight reduction of the maximum rate of pressure rise when SOI_p is significantly advanced.

In Figs. 17 and 18, the effect of injection timing on NO_x concentration at the exhaust is represented for different values of syngas fueling rates. Comparing the two figures, the effect of the variation of injection pressure of pilot injection can be highlighted. NO_x levels exhibit an increasing-decreasing behavior with retarding the injection for all values of syngas rate and injection pressure. This behavior is also confirmed by data reported for dual-fuel combustion [8,13,22,28]. Referring to data already present in literature, it could be argued that a further increase of SOI_p would have led to a further decrease of NO_x levels. However, these tests have not been performed in this study

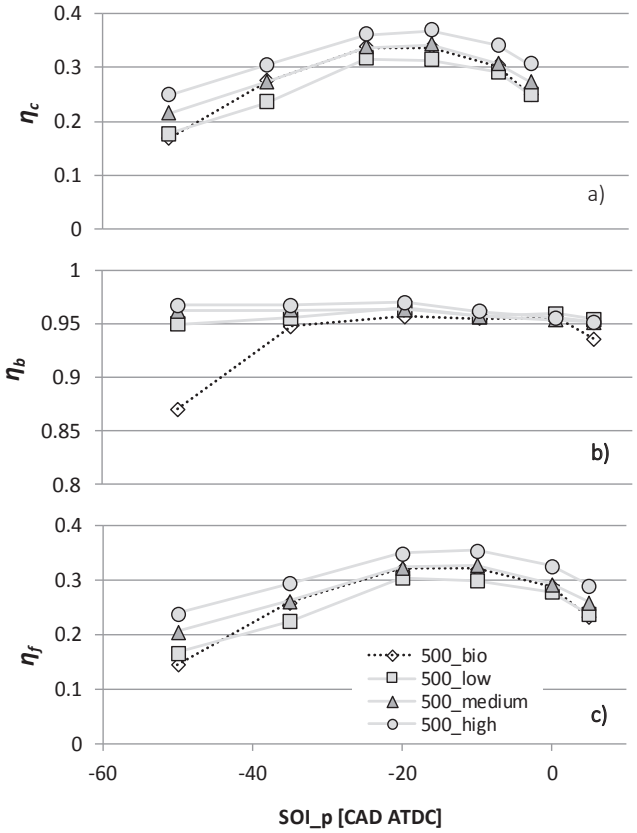

Fig. 11. Thermal Efficiency (a), Combustion Efficiency (b) and Fuel Conversion Efficiency (c) versus pilot injection timing for different syngas fueling rates with: p_rail = 500 bar, 1500 rpm, p_{in} = 129 kPa, T_{in} = 28 °C, Q_p = 11 mm^3/cycle.

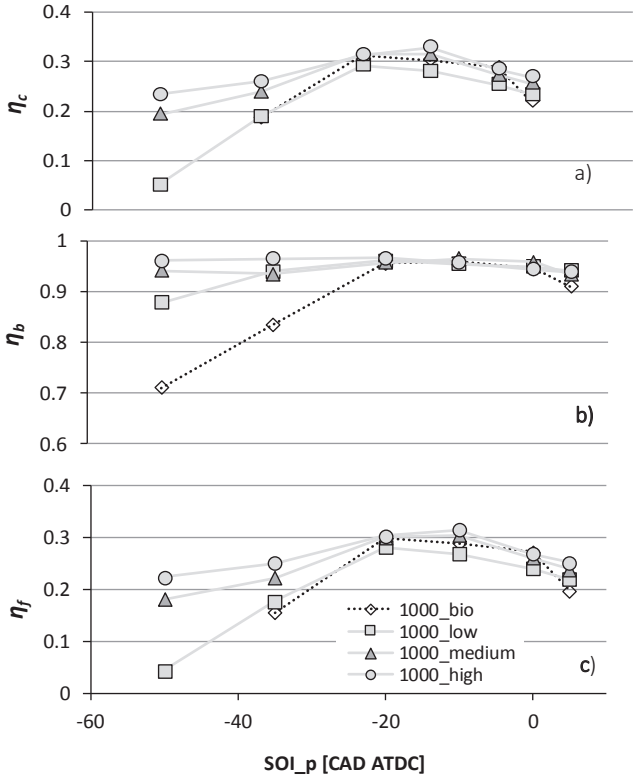

Fig. 12. Thermal Efficiency (a), Combustion Efficiency (b) and Fuel Conversion Efficiency (c) versus pilot injection timing for different syngas fueling rates with: p_rail = 1000 bar, 1500 rpm, p_{in} = 129 kPa, T_{in} = 28 °C, Q_p = 11 mm^3/cycle.

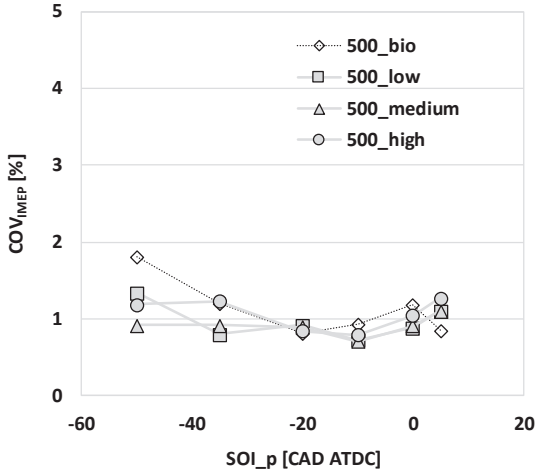

Fig. 13. COV of IMEP versus pilot injection timing for different syngas fueling rates with: p_rail = 500 bar, 1500 rpm, p_{in} = 129 kPa, T_{in} = 28 °C, Q_p = 11 mm^3/cycle.

since, as already shown In Figs. 11 and 12, this would lead to an unacceptable reduction in overall efficiency.

The overleaning of the biodiesel/air/gaseous fuel mixture deriving from a very advanced pilot injection is at the basis of this behavior (as already described in [6]). The injection pressure of the liquid fuel plays a key role in decreasing NO_x concentration at the exhaust. For injections close to TDC, an increase of injection pressure leads, as expected, to a limited increase of NO_x levels. However, a higher value of p_rail (Fig. 18) leads to a drastic reduction of NO_x advancing pilot injection more than −20 CAD ATDC; a lower injection pressure (Fig. 17) determines a similar reduction only advancing pilot injection more than −40 CAD ATDC. Still in this case, this behavior can be explained considering that a higher injection pressure determines smaller

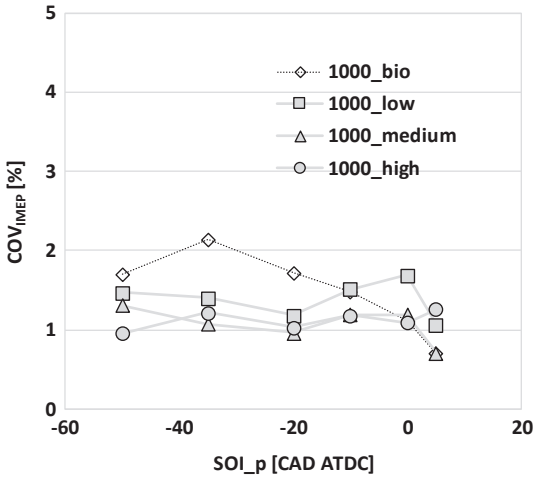

Fig. 14. COV of IMEP versus pilot injection timing for different syngas fueling rates with: p_rail = 1000 bar, 1500 rpm, p_{in} = 129 kPa, T_{in} = 28 °C, Q_p = 11 mm^3/cycle.

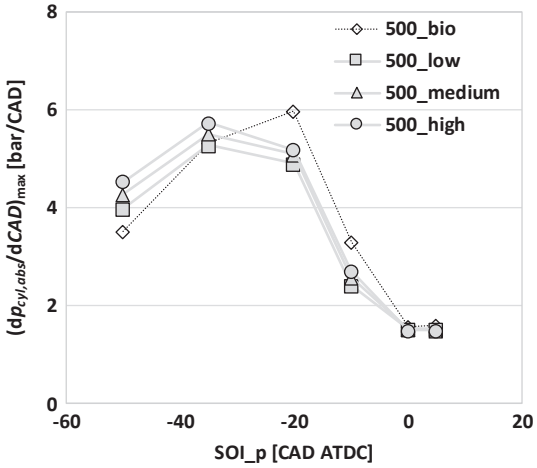

Fig. 15. Peak of cylinder pressure rise rate versus pilot injection timing for different syngas fueling rates with: p_rail = 500 bar, 1500 rpm, pin = 129 kPa, Tin = 28 °C, Q_p = 11 mm^3/cycle.

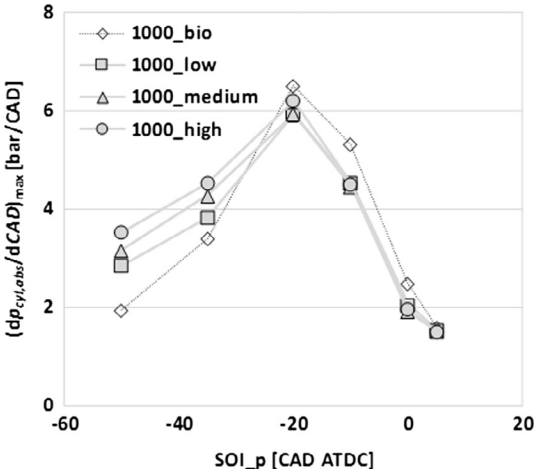

Fig. 16. Peak of cylinder pressure rise rate versus pilot injection timing for different syngas fueling rates with: p_rail = 1000 bar, 1500 rpm, p_{in} = 129 kPa, T_{in} = 28 °C, Q_p = 11 mm^3/cycle.

droplets, then a faster and more complete atomization taking into account the long ignition delay. All these phenomena lead to a more homogeneous combustion and therefore to lower local temperatures.

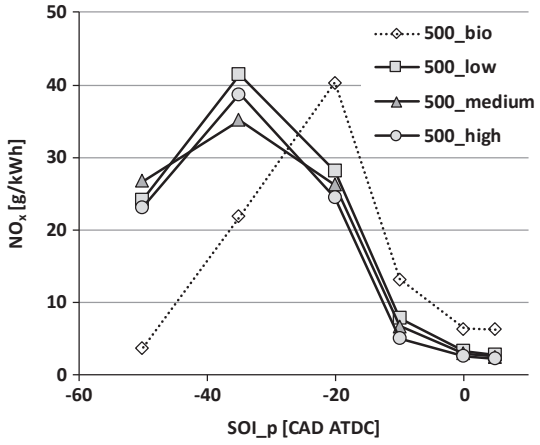

Fig. 17. NO_x emissions versus pilot injection timing for different syngas fueling rates: 1500 rpm, p_{in} = 129 kPa, T_{in} = 28 °C, Q_p = 11 mm^3/cycle, p_rail = 500 bar.

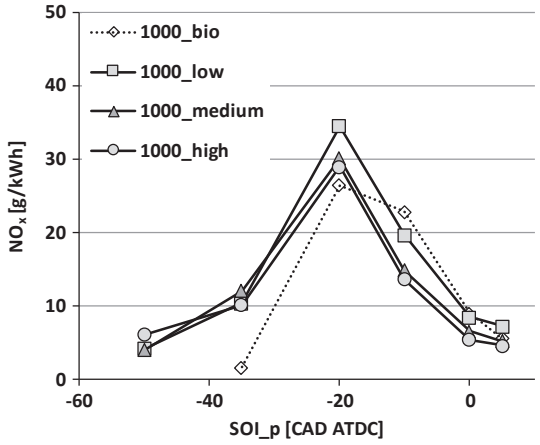

Fig. 18. NO_x emissions versus pilot injection timing for different syngas fueling rates: 1500 rpm, p_{in} = 129 kPa, T_{in} = 28 °C, Q_p = 11 mm^3/cycle, p_rail = 1000 bar.

From the two figures it is also possible to highlight that the presence of a syngas in variable amount has a secondary effect on NO_x levels, mainly consisting in a shift of NO_x levels deriving from the combustion without syngas towards more advanced pilot injections. This result can be determined by the combustion behavior already analyzed in Figs. 7 and 8, from which it was highlighted that, with syngas, the peak of HRR is advanced without varying significantly the related crank angle. NO_x emission levels follow the same behavior, being mainly affected by the temperature reached during combustion, function of the heat release rate.

In Figs. 19 and 20, the effect of injection timing on THC concentration at the exhaust is represented for different values of syngas fueling rates. Comparing the two figures, the effect of the variation of injection pressure of pilot injection can be highlighted. Similarly to what reported in [25], the behavior of THC is characterized by a first decreasing trend associated to a variation of injection timing from high to intermediate advance; then a slow increase is observed, from intermediate to retarded timing. The tendency of fuel droplets to spread in all the combustion chamber, in particular close to the cylinder liner, as a result of long ignition delay associated to very advanced injections (see also Figs. 5 and 6) is at the basis of this behavior. Increasing injection pressure determines a pilot spray more spread and shorter (see Fig. 2). This, in turn, contributes in further overleaning the mixture, so determining THC emissions higher than using a lower injection pressure. From the two figures it is also possible to highlight that the presence of a syngas in variable amount determines a significant reduction of THC levels only at very advanced or very retarded pilot injections; moreover, the amount of syngas trapped into the cylinder has a secondary effect on THC levels.

In Figs. 21 and 22, the effect of injection timing on CO concentration at the exhaust is represented for different values of syngas load. Comparing the two figures, the effect of the variation of injection pressure of pilot injection can be highlighted.

CO oxidation is promoted by the presence of OH radicals, which form in high temperature regions. Sjoberg and Dec in [38] showed that, for complete oxidation of CO to CO_2, local temperatures of at least 1500 K are needed under homogeneous conditions, along with the availability of OH radicals and sufficient residence time at these high temperatures. The calculation of bulk temperature using the equation of state of ideal gases and cylinder pressure acquisitions shows that the highest cylinder temperature estimated in the whole experimental campaign barely reaches 1000 K, due to the high dilution of mixture and to the low lower heating value of syngas. Moreover, maximum cylinder temperature tends to decrease either advancing or retarding pilot injection. This explains the observed behavior of CO emission levels.

From the two figures it can be highlighted that the presence of a syngas in variable amount determines a sensible increase in CO retarding the pilot injections, while, when it is advanced, CO levels with syngas are lower. Moreover, the amount of syngas trapped into the cylinder has a significant effect on CO levels: when the pilot injection is advanced, CO levels increase as the syngas amount decreases, while the effect is opposite as the pilot injection is retarded. This behavior can be observed with both low and high injection pressure. Trends discussed in this session have been also reported in other works [8,39].

3.3. Effect of biodiesel injection splitting

As previously shown, the absolute values of the fuel conversion efficiency are low. Since the low efficiency and high emission levels are supposingly due to the poor combustion determined by the syngas, characterized by a low calorific value, splitting the pilot injection has been tested as a way to sustain the syngas combustion [6]. Preliminary results have already demonstrated that the different behavior of the combustion with split injections has a significant influence also on tailpipe emissions: fuel conversion efficiency values and CO and THC levels at tailpipe indicate that for intermediate values (between 10 and 30 CAD) of dwell between the two pilot injections the combustion of the fuel trapped into the cylinder is more complete; NO_x emissions confirm this evidence, exhibiting higher levels usually associated to a high heat release rate. Therefore, the role of injection parameters, as well as the amount of syngas into the cylinder, requires a deeper study in order to be fully understood with the aim of further reduce fuel

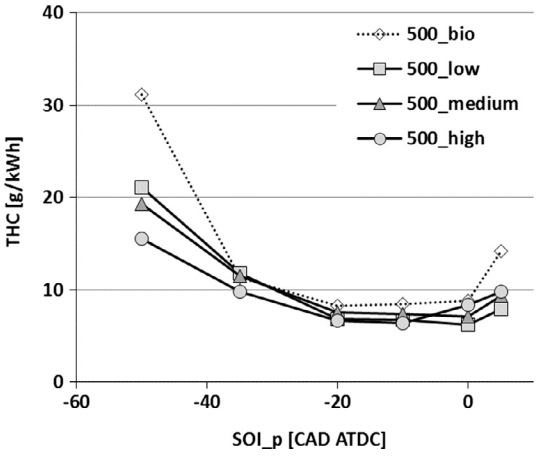

Fig. 19. THC emissions versus pilot injection timing for different syngas fueling rates: 1500 rpm, p_{in} = 129 kPa, T_{in} = 28 °C, Q_p = 11 mm^3/cycle, p_rail = 500 bar.

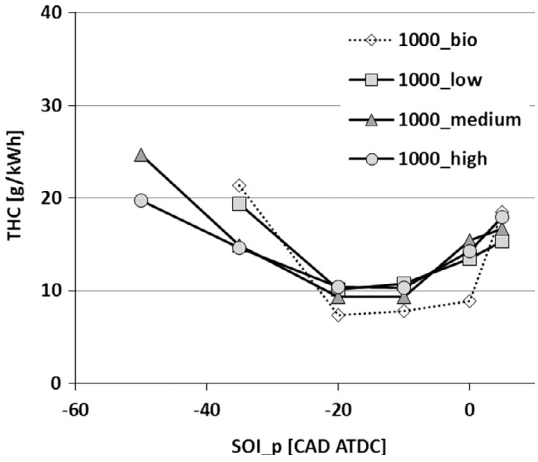

Fig. 20. THC emissions versus pilot injection timing for different syngas fueling rates: 1500 rpm, p_{in} = 129 kPa, T_{in} = 28 °C, Q_p = 11 mm^3/cycle, p_rail = 1000 bar.

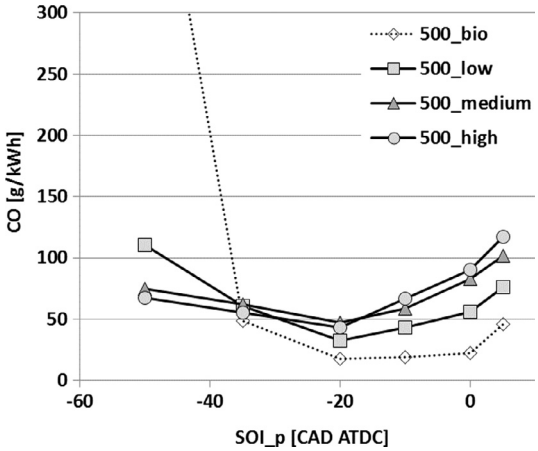

Fig. 21. CO emissions versus pilot injection timing for different syngas fueling rates: 1500 rpm, p_{in} = 129 kPa, T_{in} = 28 °C, Q_p = 11 mm^3/cycle, p_rail = 500 bar.

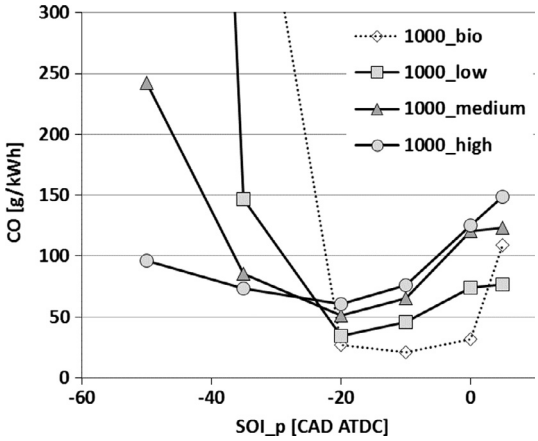

Fig. 22. CO emissions versus pilot injection timing for different syngas fueling rates: 1500 rpm, p_{in} = 129 kPa, T_{in} = 28 °C, Q_p = 11 mm^3/cycle, p_rail = 1000 bar.

consumption and pollutant emissions levels. In this section, the effect of pilot injection pressure and the syngas fueling rate will be analyzed based on a second experimental campaign in which the injection of pilot fuel has been split.

In Figs. 23 and 24, the HRR histories are reported, obtained when two split injections, respectively at 500 and 1000 bar, are operated; the first injection was always characterized by a timing of −35 CAD ATDC, while the dwell between the beginning of the two injections was varied in the range 15 ÷ 45 CAD. For comparison purposes, also the HRR behavior obtained with only one pilot injection, injected with a timing equal to the one characterizing the first split injection, is reported.

Increasing the injection pressure, it can be seen that: when the dwell between the two injections is low (equal to 15 CAD in the case of −35 and −20 CAD ATDC respectively for first and second split injections) the HRR related to the two injections cannot be distinguished in this case as well: only one premixed heat release phase is observed with a higher peak compared to the previous case. Increasing the dwell between the two injections, on the contrary, a two-phases HRR is clearly visible. The first phase of the combustion is not significantly different if compared to the first phase observed with the lower injection pressure. The second peak of combustion, in this case too, first decreases and then increases with the longer dwell between the two injections, but it is characterized by a higher value and a premixed-like behavior if compared to the corresponding observed at lower injection pressure.

The described combustion development determines different values of the fuel conversion efficiency. In particular, in Figs. 25 and 26 the value of fuel conversion efficiency η_f referred to the indicated power as a function of dwell between the two split injections for different injection timings of the first split injection are reported (in black) respectively for p_rail equal to 500 and 1000 bar. In order to compare the fuel conversion efficiency η_f between single and split injections, the value of the fuel conversion efficiency η_f related to the single pilot injection (in grey) is plot on the same figures. It is possible to note that, increasing the dwell, η_f first increases and then decreases. Furthermore, it is highlighted that splitting the pilot injection always leads to an increase of η_f. It is possible to note that η_f increases whatever first injection timing and dwell compared to the single injection.

For both p_rail values, the highest η_f values are observed for a dwell of 20 CAD. Moreover, increasing p_rail (Fig. 26) leads to an overall increase of η_f; in particular, the maximum value is increased from 20% up to 25%.

In Figs. 27 and 28, COV_{IMEP} as a function of dwell between the two split injections for different injection timings of the first split injection are reported (in black) respectively for p_rail equal to 500 and 1000 bar. In order to compare the COV_{IMEP} between single and split injections, the value of the COV_{IMEP} related to the single pilot injection (in grey) is plot on the same figures. The results, shown with low syngas fueling level but representing those obtained with medium and high levels, demonstrate, on one hand, that dwell has no fundamental effect on COV_{IMEP}; on the other hand, increasing p_rail, COV_{IMEP} does not vary significantly; a slight increase is observed when the dwell is around 5–10 CAD, probably due to the low repeatability of injection

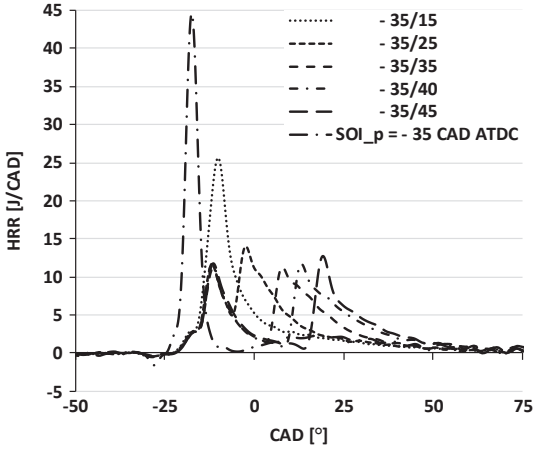

Fig. 23. Heat Release Rate versus crank angle for different dwells between the two split injections with SOI = −35 CAD ATDC and p_rail = 500 bar: 1500 rpm, p_{in} = 129 kPa, T_{in} = 28 °C, Q_p = 11 mm^3/cycle (medium syngas fueling rate).

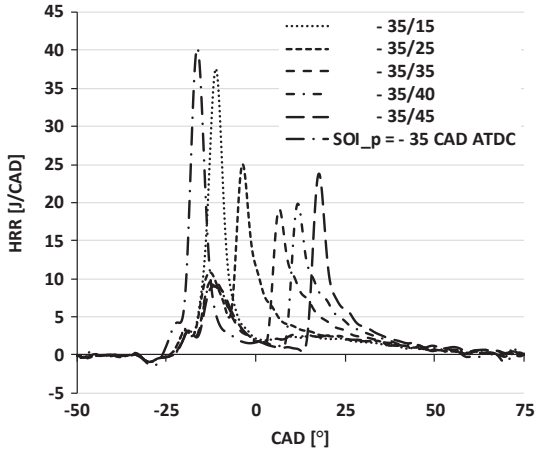

Fig. 24. Heat Release Rate versus crank angle for different dwells between the two split injections with SOI = −35 CAD ATDC and p_rail = 1000 bar: 1500 rpm, p_{in} = 129 kPa, T_{in} = 28 °C, Q_p = 11 mm^3/cycle (medium syngas fueling rate).

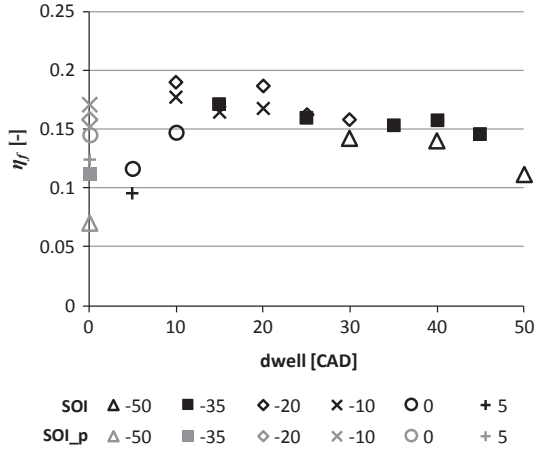

Fig. 25. Fuel conversion efficiency referred to the indicated power versus dwell between first and second split injections for different first split injection timings (SOI) with p_rail = 500 bar and comparison with pilot injection results: 1500 rpm, p_{in} = 129 kPa, T_{in} = 28 °C, Q_p = 11 mm^3/cycle (low syngas fueling rate).

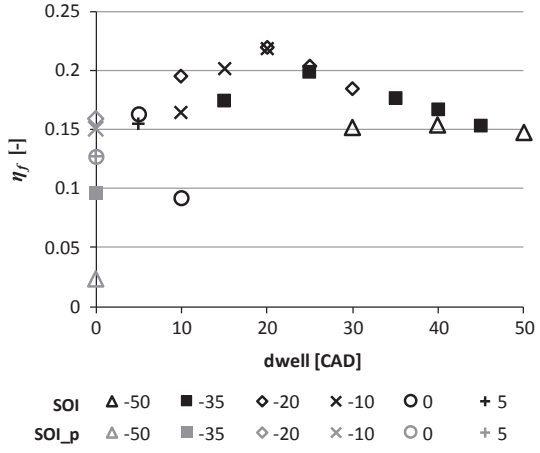

Fig. 26. Fuel conversion efficiency referred to the indicated power versus dwell between first and second split injections for different first split injection timings (SOI) with p_rail = 1000 bar and comparison with pilot injection results: 1500 rpm, p_{in} = 129 kPa, T_{in} = 28 °C, Q_p = 11 mm^3/cycle (low syngas fueling rate).

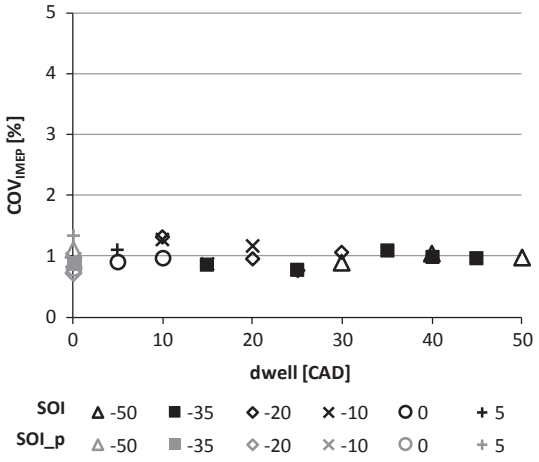

Fig. 27. COV of IMEP versus dwell between first and second split injections for different first split injection timings (SOI) with p_rail = 500 bar and comparison with pilot injection results: 1500 rpm, p_{in} = 129 kPa, T_{in} = 28 °C, Q_p = 11 mm^3/cycle (low syngas fueling rate).

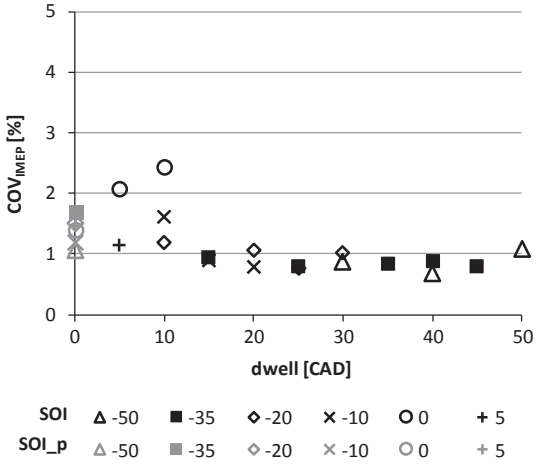

Fig. 28. COV of IMEP versus dwell between first and second split injections for different first split injection timings (SOI) with p_rail = 1000 bar and comparison with pilot injection results: 1500 rpm, p_{in} = 129 kPa, T_{in} = 28 °C, Q_p = 11 mm^3/cycle (low syngas fueling rate).

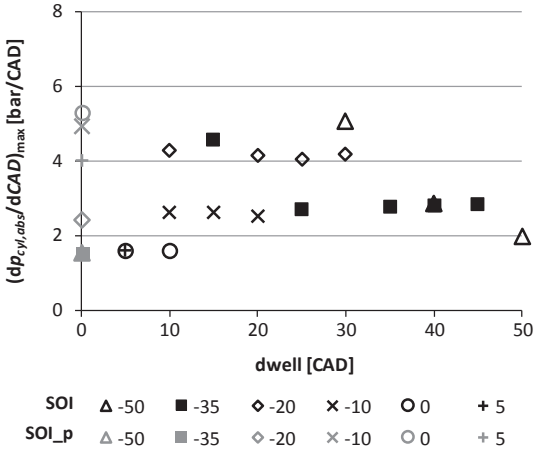

Fig. 29. Peak of cylinder pressure rise rate versus dwell between first and second split injections for different first split injection timings (SOI) with p_rail = 500 bar and comparison with pilot injection results: 1500 rpm, p_{in} = 129 kPa, T_{in} = 28 °C, Q_p = 11 mm^3/cycle (low syngas fueling rate).

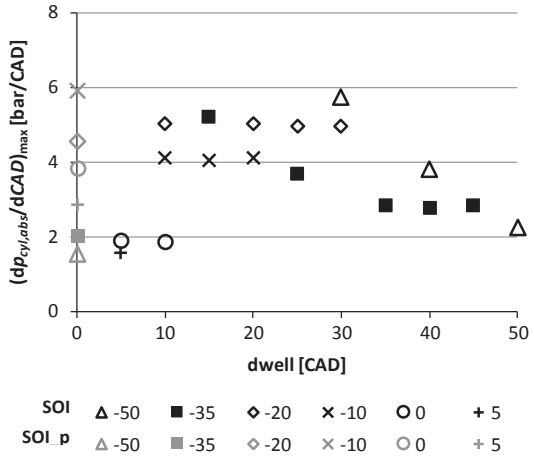

Fig. 30. Peak of cylinder pressure rise rate versus dwell between first and second split injections for different first split injection timings (SOI) with p_rail = 1000 bar and comparison with pilot injection results: 1500 rpm, p_{in} = 129 kPa, T_{in} = 28 °C, Q_p = 11 mm^3/cycle (low syngas fueling rate).

event performing two close injections.

In Figs. 29 and 30, $(dp_{cyl,abs}/dCAD)_{max}$ as a function of dwell between the two split injections for different injection timings of the first split injection are reported (in black) respectively for p_rail equal to 500 and 1000 bar. In order to compare the $(dp_{cyl,abs}/dCAD)_{max}$ between single and split injections, the value of the $(dp_{cyl,abs}/dCAD)_{max}$ related to the single pilot injection (in grey) is plot on the same figures. The results, shown with low syngas fueling level but representing those obtained with medium and high levels, demonstrate that peak of pressure rise rate is affected by injection splitting depending on SOI and dwell; for retarded SOI (−10, 0 and +5 CAD ATDC) peak of pressure rise rate is decreased whatever the dwell; for advanced SOI (−20, −35, −50 CAD ATDC) peak of pressure rise rate is increased, with this increased more pronounced using intermediate values of dwell (10 ÷ 40 CAD).

In Figs. 31 and 32, NO_x emission data versus dwell between first and second split injection for different injection timings are compared respectively for p_rail equal to 500 and 1000 bar. In order to compare NO_x emission data between single and split injection, NO_x values related to the single pilot injection (in grey) are plot on the same figures.

The general trend indicates that NO_x levels first increase and then decrease increasing the dwell between the two split injections. For both p_rail values, the highest NO_x levels are observed for a dwell ranging between 10 and 30 CAD, coincident with the range in which the highest fuel conversion efficiency has been observed. Moreover, increasing p_rail (Fig. 32) leads to an overall increase of NO_x levels, this experimental observation being due to the higher rate of heat release determined splitting the pilot injection, as already observed in Figs. 23 and 24. Referring to Fig. 31, it is visible that splitting the pilot injection leads to a decrease of NO_x levels whatever the first injection timing and the dwell are. Increasing p_rail (Fig. 32), the split injection determines a reduction on NO_x levels only when intermediate first injection timings (−20 and −10 CAD ATDC) are used; in all the other cases, splitting the pilot injection determines an increase of NO_x levels.

In Figs. 33 and 34, THC emission data versus dwell between first and second split injections for different injection timings are compared respectively for p_rail equal to 500 and 1000 bar. In order to compare the THC emission levels between single and splitting injection, THC levels related to the single pilot injection (in grey) are plot on the same figures (please note that THC level measured with p_rail = 1000 bar and a single pilot injection timing equal to −50 CAD ATDC is not reported in the figure because too high, equal to 103 g/kWh).

It is possible to note that, increasing the dwell, THC levels first decrease and then increase. Furthermore, it has been highlighted that the lowest THC levels observed is for a dwell ranging between 10 and 30 CAD coincident with the range in which the highest fuel conversion efficiency has been observed. Moreover, increasing p_rail (Fig. 34) leads to an overall increase of THC levels.

It is possible to note that THC levels decrease whatever first injection timing and dwell compared to the single injection.

Results comparable to those observed for THC emissions have been observed for CO emissions; i.e. first decreasing and then increasing with increasing dwell. In Figs. 35 and 36, CO emissions versus dwell between first and second split injections are reported for different injection timings, respectively for p_rail equal to 500 and 1000 bar. In Fig. 36, CO level measured performing a single pilot injection with SOI_p equal to −50 CAD ATDC is not reported because too high, equal to 1880 g/kWh. Furthermore, it has been highlighted, also for CO, that the lowest CO levels observed is for a dwell ranging between 10 and 30 CAD for both p_rail values. Moreover, increasing p_rail (Fig. 36) leads to an overall decrease of CO levels.

Summarizing, results previously shown allow to argue that the injection splitting is an effective way for sustaining the gaseous fuel combustion at low loads in dual-fuel engines combustion. Its beneficial effect, resulting in an increase of η_f and a reduction on THC, NO_x and CO emission levels compared to the single injection strategy, can be obtained only properly tuning the timing of both injections. Injection pressure also plays a key role; interestingly, its effect on regulated gaseous emissions is beneficial if set at lower values, given the particular dynamics of atomization, diffusion and vaporization associated to small (pilot) injections.

4. Conclusions

In this work, the improvements in the combustion development at low loads deriving from the splitting of the liquid fuel injection have been assessed on a common-rail injection, single-cylinder research diesel engine equipped with a high pressure common rail injection system and operated in dual-fuel mode. In this case, a synthetic producer gas was used as inducted gaseous fuel, while biodiesel was used as pilot fuel.

Initially, the spray morphology was characterized in a constant-volume vessel for different values of injection duration and pressure, as well as vessel backpressure.

Then, the experimental campaign run on the engine was divided in two sessions. During the former, only one pilot injection of constant fuel amount was performed, while the rail pressure and injection timing were varied together with the amount of gaseous fuel trapped in the cylinder. During the latter, the pilot injection was split in two smaller injections and the effect of the dwell between them was investigated as

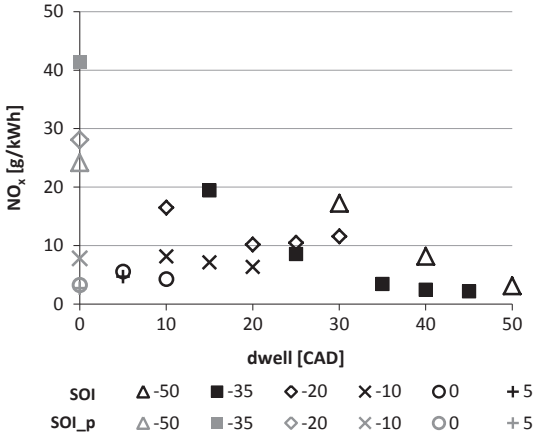

Fig. 31. NO_x emissions versus dwell between first and second split injection for different first split injection timings (SOI) with p_rail = 500 bar and comparison with pilot injection results: 1500 rpm, p_{in} = 129 kPa, T_{in} = 28 °C, Q_p = 11 mm^3/cycle (low syngas fueling rate).

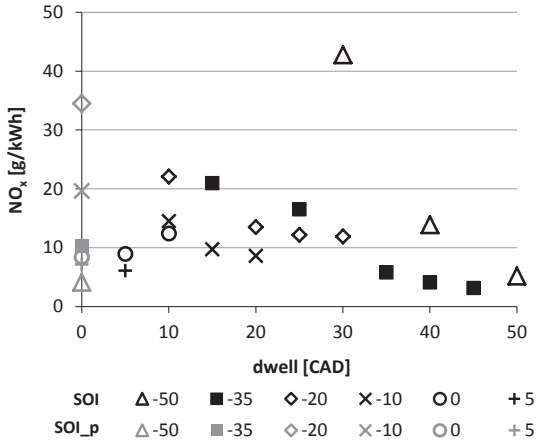

Fig. 32. NO_x emissions versus dwell between first and second split injection for different first split injection timings (SOI) with p_rail = 1000 bar and comparison with pilot injection results: 1500 rpm, p_{in} = 129 kPa, T_{in} = 28 °C, Q_p = 11 mm^3/cycle (low syngas fueling rate).

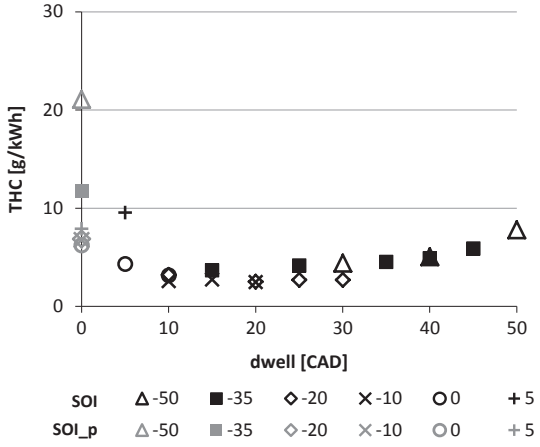

Fig. 33. THC emissions versus dwell between first and second split injection for different first split injection timings (SOI) with p_rail = 500 bar and comparison with pilot injection results: 1500 rpm, p_{in} = 129 kPa, T_{in} = 28 °C, Q_p = 11 mm^3/cycle (low syngas fueling rate).

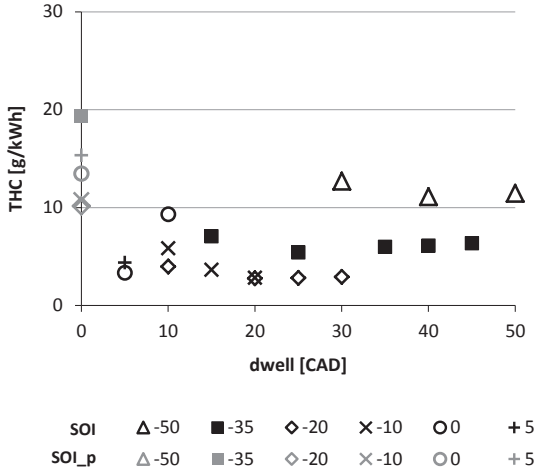

Fig. 34. THC emissions versus dwell between first and second split injection for different first split injection timings (SOI) with p_rail = 1000 bar and comparison with pilot injection results: 1500 rpm, p_{in} = 129 kPa, T_{in} = 28 °C, Q_p = 11 mm^3/cycle (low syngas fueling rate).

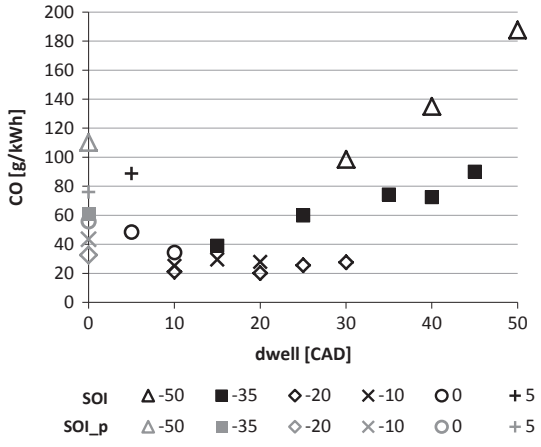

Fig. 35. CO emissions versus dwell between first and second split injection for different first split injection timings (SOI) with p_rail = 500 bar and comparison with pilot injection results: 1500 rpm, p_{in} = 129 kPa, T_{in} = 28 °C, Q_p = 11 mm^3/cycle (low syngas fueling rate).

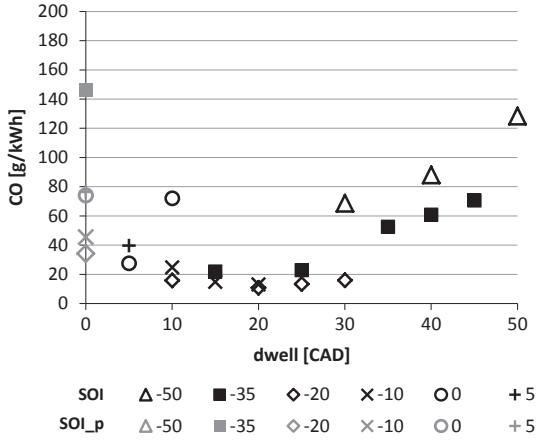

Fig. 36. CO emissions versus dwell between first and second split injection for different first split injection timings (SOI) with p_rail = 1000 bar and comparison with pilot injection results: 1500 rpm, p_{in} = 129 kPa, T_{in} = 28 °C, Q_p = 11 mm^3/cycle (low syngas fueling rate).

well.

The results of the first set of experiments revealed that pilot injection timing and pressure both affect the combustion development. This resulted in sensible variations on thermal and combustion efficiencies, and therefore on fuel conversion efficiency, the last one exhibiting maximum values with pilot injection timing is slightly advanced respect to top dead center and lower injection pressure. In these conditions, total hydrocarbons and carbon monoxide were lowered, while nitric oxides were increased. The amount of gas demonstrated to have a secondary effect on combustion development and emissions levels at the exhaust.

Splitting pilot injection, demonstrated to be an effective way to increase fuel conversion efficiency and to reduce the levels of all the pollutant species compared to the single pilot injection strategy with the engine operating at low loads. Based on the extensive experimental activity described in the paper, a dwell ranging between 10 and 30 degrees of crank angle, combined with a first injection timing ranging between 35 and 20 degrees of crank angle before top dead center guarantee the highest fuel conversion efficiency and the lowest pollutants emission levels. Injection pressure confirmed to be a significant factor in affecting the combustion development, while a secondary effect was determined by the gaseous mass inducted in the cylinder.

Summarizing, results previously shown allow to argue that the

injection splitting is an effective way for sustaining the gaseous fuel combustion in dual-fuel engines, operating at low loads. Its beneficial effect, resulting in an increase of η_f and a reduction on THC, NO_x and CO emission levels compared to the single injection strategy, can be obtained only properly tuning the timing of both injections. Injection pressure also plays a key role; interestingly, its effect on regulated gaseous emissions is beneficial if set at lower values, given the particular dynamics of atomization, diffusion and vaporization associated to small (pilot) injections.

Acknowledgements

The Author wishes to thank Mr. Andrea Riso, Dr. Cristian Leucci and Dr. Francesco Liquori for their fundamental contribution to the present work, in particular during the experiments conducted for the spray characterization in the constant-volume vessel.

References

[1] McKendry P. Energy production from biomass (part 2): conversion technologies. Bioresource Technol 2002;83:47–54.
[2] Martinez JD, Mahkamov K, Andrade RV, Silva Lora EE. Syngas production in downdraft biomass gasifiers and its application using internal combustion engines. Renew Energ 2012;38:1–9.
[3] Orbaiz P, Brear MJ, Abbasi P, Dennis PA. A Comparative Study of a Spark Ignition Engine Running on Hydrogen, Synthesis Gas and Natural Gas. SAE Technical Paper 2013–01-0229.
[4] Bhaduri S, Contino F, Jeanmart H, Breuer E. The effects of biomass syngas composition, moisture, tar loading and operating conditions on the combustion of a tar-tolerant HCCI (Homogeneous Charge Compression Ignition) engine. Energy 2015;87:289–302.
[5] Dhole AE, Yarasu RB, Lata DB, Priyam A. Effect on performance and emissions of a dual fuel diesel engine using hydrogen and producer gas as secondary fuels. Int J Hydrogen Energ 2014;39:8087–97.
[6] Carlucci AP, Ficarella A, Laforgia D. Potentialities of common rail injection system for the control of dual fuel biodiesel-producer gas combustion and emissions. J Energ Eng-ASCE 2014;140. A4014011-1 — A4014011-8 (DOI: 10.1061/(ASCE)EY.1943-7897.0000150) ISSN: 0733-9402.
[7] Carlucci AP, Colangelo G, Ficarella A, Laforgia D, Strafella L. Improvements in dual-fuel biodiesel-producer gas combustion at low load through pilot injection splitting. J Energ Eng-ASCE 2015;141. C4014006–1 – C4014006–8 (DOI: 10.1061/(ASCE)EY.1943-7897.0000231) ISSN: 0733-9402.
[8] Hernandez JJ, Lapuerta M, Barba J. Effect of partial replacement of diesel or biodiesel with gas from biomass gasification in a diesel engine. Energy 2015;89:148–57.
[9] Ramadhas AS, Jayaraj S, Muraleedharan C. Dual fuel mode operation in diesel engines using renewable fuels: Rubber seed oil and coir-pith producer gas. Renew Energ 2008;33:2077–83.
[10] Hernàndez JJ, Lapuerta M, Barba J. Separate effect of H_2, CH_4 and CO on diesel engine performance and emissions under partial diesel fuel replacement. Fuel 2016;165:173–84.
[11] Sahoo BB, Sahoo N, Saha UK. Effect of H_2:CO ratio in syngas on the performance of a dual fuel diesel engine operation. Appl Therm Eng 2012;49:139–46.
[12] Costa M, La Villetta M, Massarotti N, Piazzullo D, Rocco V. Numerical analysis of a compression ignition engine powered in the dual-fuel mode with syngas and biodiesel. Energy 2017. http://dx.doi.org/10.2016/j.energy.2017.02.160.
[13] Roy MM, Tomita E, Kawahara N, Harada Y, Sakane A. Performance and emission comparison of a supercharged dual-fuel engine fueled by producer gases with varying hydrogen content. Int J Hydrogen Energ 2009;34:7811–22.
[14] Banapumarth NR, Tewari PG, Hosmath RS. Experimental investigations of a four-stroke single cylinder direct injection diesel engine operated on dual fuel mode with producer gas as inducted fuel and Honge oil and its methyl ester (HOME) as injected fuels. Renew Energ 2008;33:2007–18.
[15] Banapumarth NR, Tewari PG, Yaliwal VS, Kambalimath S, Basavarajappa YH. Combustion characteristics of a 4-stroke CI engine operated on Honge oil, Neem and Rice Bran oils when directly injected and dual fuelled with producer gas induction. Renew Energ 2009;34:1877–84.
[16] Singh RN, Singh SP, Pathak BS. Investigations on operation of CI engine using producer gas and rice bran oil in mixed fuel mode. Renew Energ 2007;32:1565–80.
[17] Rinaldini CA, Allesina G, Pedrazzi S, Mattarelli E, Savioli T, Morselli N, et al. Experimental investigation on a Common Rail Diesel engine partially fueled by syngas. Energ Convers Manage 2017;138:526–37.
[18] Papagiannakis RG, Rakopoulos CD, Hountalas DT, Rakopoulos DC. Emission characteristics of high speed, dual fuel, compression ignition engine operating in a wide range of natural gas/diesel fuel proportions. Fuel 2010;89:1397–406.
[19] Krishnan SR, Srinivasan KK, Raihan MS. The effect of injection parameters and boost pressure on diesel-propane dual fuel low temperature combustion in a single-cylinder research engine. Fuel 2016;184:490–502.
[20] Pan W, Yao C, Han G, Wei H, Wang Q. The impact of intake air temperature on performance and exhaust emissions of a diesel methanol dual fuel engine. Fuel 2015;162:101–10.
[21] Papagiannakis RG. Study of air inlet preheating and EGR impacts for improving the operation of compression ignition engine running under dual fuel mode. Energ Convers Manage 2013;68:40–53.
[22] Wang Z, Zhao Z, Wang D, Tan M, Han Y, Liu Z, et al. Impact of pilot diesel ignition mode on combustion and emissions characteristics of a diesel/natural gas dual fuel heavy-duty engine. Fuel 2016;167:248–56.
[23] Aksu C, Kawahara N, Tsuboi K, Kondo M, Tomita E. Extension of PREMIER combustion operation range using split micro pilot fuel injection in a dual fuel natural gas compression ignition engine: a performance-based and visual investigation. Fuel 2016;185:243–53.
[24] Carlucci AP, Ficarella A, Laforgia D. Effects of pilot injection parameters on combustion for common rail diesel engines. SAE Paper 2003–01-0700.
[25] Singh S, Krishnan SR, Srinivasan KK, Midkiff KC, Bell SR. Effect of pilot injection timing, pilot quantity and intake charge conditions on performance and emissions for an advanced low-pilot-ignited natural gas engine. Int J Engine Res 2004;5:329–48.
[26] Carlucci AP, Ficarella A, Laforgia D. Control of the combustion behaviour in a diesel engine using early injection and gas addition. Appl Therm Eng 2006;26:2279–86.
[27] Carlucci AP, de Risi A, Laforgia D, Naccarato F. Experimental investigation and combustion analysis of a direct injection dual-fuel diesel-natural gas engine. Energy 2008;33:256–63.
[28] Sahoo BB, Sahoo N, Saha UK. Effect of engine parameters and type of gaseous fuel on the performance of dual-fuel gas diesel engines - a critical review. Renew Sust Energ Rev 2009;13:1151–84.
[29] Carlucci AP, Laforgia D, Saracino R, Toto G. Combustion and emissions control in diesel–methane dual fuel engines: the effects of methane supply method combined with variable in-cylinder charge bulk motion. Energ Convers Manage 2011;52:3004–17.
[30] Carlucci AP, D'Amico L, De Domenico S, Ficarella A, Santino A, Strafella L, et al. Biodiesel production from Cynara Cardunculus L. and Brassica Carinata A. Braun seeds and their suitability as fuels in compression ignition engines. Ital J Agron 2016;11:47–56. http://dx.doi.org/10.4081/ija.2016.685.
[31] Cai A, Carlucci AP, Colangelo G, de Luca A, de Giorgi M, Minosi G, et al. Analisi e studi relativi all'ottimizzazione di un impianto di gassificazione e cogenerazione a biomasse lignocellulosiche. Proc. 64° Congresso Nazionale ATI 2009, L'Aquila (ITALY).
[32] Woschni G. A universally applicable equation for the instantaneous heat transfer coefficient in the internal combustion engines. SAE Paper 670937, 1967.
[33] Nehmer DA, Reitz RD. Measurement of the Effect of Injection Rate and Split Injections on Diesel Engine Soot and NOx Emissions. SAE Technical Paper 940668.
[34] Ricart LM, Reitz RD. Visualization and Modeling of Pilot Injection and Combustion in Diesel Engines. SAE Technical Paper 960833.
[35] Uludogan A, Xin J, Reitz RD. Exploring the Use of Multiple Injectors and Split Injections to Reduce DI Diesel Engine Emissions. SAE Technical Paper 962058.
[36] Bower GR, Foster DE. The Effect of Split Injection on Fuel Distribution in an Engine-Fed Combustion Chamber. SAE Technical Paper 930864.
[37] Siebers D. Liquid-Phase Fuel Penetration in Diesel Sprays. SAE Technical Paper 980809.
[38] Sjöberg M, Dec JE. An investigation into lowest acceptable combustion temperatures for hydrocarbon fuels in HCCI engines. P Combust Inst 2005;30:2719–26.
[39] Christodoulou F, Megaritis A. The effect of reformer gas mixture on the performance and emissions of an HSDI diesel engine. Int J Hydrogen Energ 2014;39:9798–808.